Graded index profiles and loss-induced single-mode characteristics in vertical-cavity surface-emitting lasers with petal-shape holey structure*

Liu An-Jin(刘安金)[a], Qu Hong-Wei(渠红伟)[a], Chen Wei(陈 微)[a], Jiang Bin(江 斌)[a], Zhou Wen-Jun(周文君)[a], Xing Ming-Xin(邢名欣)[a], and Zheng Wan-Hua(郑婉华)[a)b)†]

[a] *Nano-optoelectronics Lab, Institute of Semiconductors, Chinese Academy of Sciences, Beijing* 100083, *China*

[b] *State Key Laboratory of Integrated Optoelectronics, Institute of Semiconductors, Chinese Academy of Sciences, Beijing* 100083, *China*

(Received 7 July 2010; revised manuscript received 29 July 2010)

The 850-nm oxide-confined vertical-cavity surface-emitting lasers with petal-shape holey structures are presented. An area-weighted average refractive index model is given to analyse their effective index profiles, and the graded index distribution in the holey region is demonstrated. The index step between the optical aperture and the holey region is obtained which is related merely to the etching depth. Four types of holey vertical-cavity surface-emitting lasers with different parameters are fabricated as well as the conventional oxide-confined vertical-cavity surface-emitting laser. Compared with the conventional oxide-confined vertical-cavity surface-emitting laser without etched holes, the holey vertical-cavity surface-emitting laser possesses an improved beam quality due to its graded index distribution, but has a lower output power, higher threshold current and lower slope efficiency. With the hole number increased, the holey vertical-cavity surface-emitting laser can realize the single-mode operation throughout the entire current range, and reduces the beam divergence further. The loss mechanism is used to explain the single-mode characteristic, and the reduced beam divergence is attributed to the shallow etching. High coupling efficiency of 86% to a multi-mode fibre is achieved for the single-mode device in the experiment.

Keywords: vertical-cavity surface-emitting lasers, single mode, low divergence angle, graded index profile

PACS: 42.55.Px, 42.60.Jf, 42.60.Pk **DOI:** 10.1088/1674-1056/20/2/024204

1. Introduction

Vertical-cavity surface-emitting lasers (abbreviated as VCSELs)[1−5] have attracted much attention due to their advantages over edge-emitting lasers, such as two-dimensional array formation, narrow circular beam, wafer level testing, and single longitudinal mode operation. However, single-mode high power VCSELs are usually demanded for a number of applications, including high-resolution high-speed laser printing,[6] optical storage,[7] position sensing,[8,9] optical interconnects,[10−12] gas detection,[13,14] atomic clock[15,16] and long-wavelength telecommunications.[17−21] Generally, there are three types of VCSELs, these being oxide-confined VCSEL,[22−24] proton-implanted VCSEL,[25−27] and tunnel junction VCSEL.[18,20,21] Among the three device structures, oxide-confined VCSEL has advantages of low power consumption, high frequency response, high uniformity, and high reliability. Hence oxide-confined VCSELs have been investigated intensively in the past years. However, for the conventional oxide-confined VCSEL, the lateral dimension is usually much larger than the effective cavity length in the longitudinal direction, and the index step between the non-oxidized region and the oxidized region is fairly large, accounting for strong optical confinement. As a result, the conventional oxide-confined VCSEL usually operates in multiple transverse modes. For example, for the 850-nm oxide-confined VCSEL, the single-mode operation is realized by reducing the oxide aperture to around 3 μm, and the output power is limited to about 3 mW.[28] However, the reduced oxide aperture causes many negative effects, such as low output power, tight fabrication tol-

*Project supported by the National Key Basic Research Special Foundation of China (Grant No. 2011CB922000), the National Natural Science Foundation of China (Grant Nos. 61025025 and 60838003), and the National High Technology Research and Development Program of China (Grant Nos. 2007AA03Z410 and 2007AA03Z408).

†Corresponding author. E-mail: whzheng@semi.ac.cn

© 2011 Chinese Physical Society and IOP Publishing Ltd

erance, and narrow modulation bandwidth.[29] These drawbacks originate from the dual roles of the oxide aperture used to confine the optical field and the injected current simultaneously, and the large index step between the oxide region and the non-oxide region.[23]

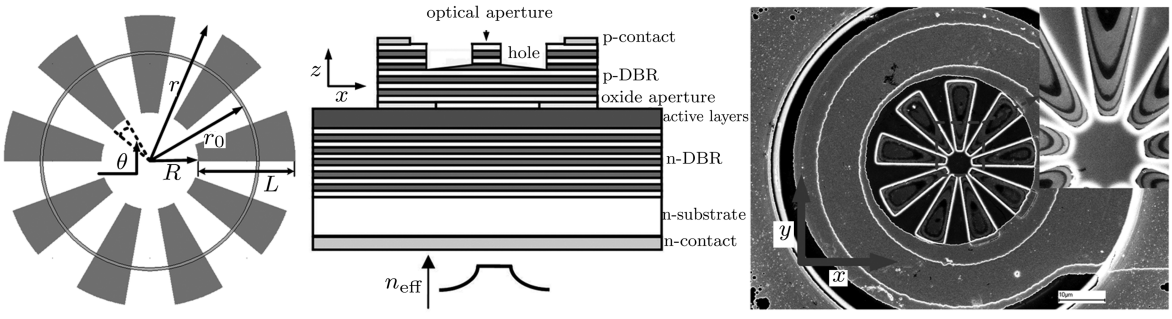
To achieve the single-mode operation with high output power in an oxide-confined VCSEL, many other methods have been proposed and developed, for example, surface relief structure,[30,31] high-index-contrast subwavelength grating structure,[32] single higher-order mode VCSEL,[33] metal aperture structure,[34] surface grating relief structure,[35] photonic crystal waveguide structure,[36−44] and mode selective aperture structure.[45−47] All the structures successfully achieve the single-mode operation due to the fact that the optical confinement is decoupled from the current confinement. The optical confinement and the current confinement are implemented separately. The oxide aperture is used merely to confine the injected current, whereas the optical field is confined by the engineered structure in the top distributed Bragg reflector (DBR). As a result, the oxide aperture can be increased to 3 μm and more, which leads to the multi-mode operation. The higher-order modes are filtered to realize the fundamental-mode operation by the engineered structure in the top DBR. This basic concept provides another degree of freedom, which can be used for the optimization of device performance, and enhances the flexibility in designing the device structure. Thus VCSELs with high performances are expected, for example, to achieve single-mode operation, high output power, low series resistance, high speed modulation, and low-divergence-angle beam.

In recent years, based on the separated confinement for the injected current and the optical field, the holey structure has also been used to achieve the single-mode operation. The oxide aperture is typically larger than the optical aperture in holey VCSEL. Furukawa *et al.*[48] first reported that they had realized the standard fundamental mode and deformed fundamental mode operations by tuning the triangular hole number and the relative position between the oxide aperture and the optical aperture in an oxide-confined VCSEL for the first time. Later, the single-mode operation was also achieved by introducing the triangular holey structure in proton-implanted VCSEL by another group,[49] and the modal characteristics were explained by the selective loss mechanism.[50] According to the selective loss mechanism, Yang *et al.*[51] reported that they had realized the single-mode high power operation in the oxide-confined VCSEL with a multi-leaf holey structure in the top DBR in 2006.

In the present paper, we demonstrate oxide-confined VCSEL with a petal-shape holey structure. The index profile of the structure is deduced from an area-weighted average refractive index model and the etching depth dependence factor. The modal characteristics are investigated in terms of the selective loss mechanism, and the high-quality beam is explained by the graded index profile and the shallow etching. Finally, the coupling efficiency to a multi-mode fibre is measured.

2. Theoretical analysis

The top view and the cross-sectional view of the device structure are illustrated in Figs. 1(a) and 1(b), respectively. The petal-shape holey pattern, which is composed of several annular-sector-shape holes, is patterned within the ring contact on the top DBR. As shown in Fig. 1(a), the region surrounded by the annular-sector-shape holes is the optical aperture for



(a) (b) (c)

Fig. 1. Schematic of the device structure. (a) Top view. The grey annular sectors represent the holes. R and r_0 denote the radii of optical aperture and oxide aperture, respectively. L refers to the height of the annular-sector-shape hole. The angle of the annular sector is given as θ in radians. (b) Cross-sectional view. The effective index profile is not scaled. (c) Scanning electron microscope (SEM) image of type C. R is 3 μm.

light emitting out. The radius of the optical aperture is given as R. The radius of the oxide aperture is r_0, which is larger than R. The total number of the annular-sector-shape holes is N The angle of each annular-sector-shape hole is given as θ in radians ($\theta = \pi/N$). The height of the annular-sector-shape hole is given as L. The refractive indices of the holey region and the semiconductor region are given as $n_{\rm a}$ and $n_{\rm s}$, respectively. All the annular-sector-shape holes share the same centre located at the central point of the optical aperture.

Indeed, the modal characteristics in this structure can be obtained numerically by standard computation techniques, for example, the full three-dimensional finite-difference time-domain (3D-FDTD) analysis.[50] However, large computation resources and huge time are always required. A simple model is used to investigate the structure in the present work. Different from the circumference-weighted average refractive index model employed in Ref. [49], an area-weighted average refractive index model is adopted here. The average refractive index is given as a function of radius r due to the symmetric structure. The effective index is roughly written in the following form:

$$n(r) = \begin{cases} n_{\rm s}, & r < R, \\ (n_{\rm a} + n_{\rm s})/2, & R < r < r_0. \end{cases} \tag{1}$$

Considering the effect of finite etching depth of the holes on the transverse index profile, the etching depth dependence factor γ was ever proposed in Ref. [52] for photonic crystal VCSELs, where $0 < \gamma < 1$. The etching depth dependence factor γ can be understood qualitatively as a relative quantity of the longitudinal optical mode which overlaps the pattern etched from the top VCSEL facet with respect to a specified depth.[52] Using a weighted average which accounts for the relative quantity of optical mode present in the etched DBR layers, then equation (1) can be rewritten as

$$n(r) = \begin{cases} n_{\rm s}, & r < R, \\ (1-\gamma)n_{\rm s} + \gamma(n_{\rm a} + n_{\rm s})/2, & R < r < r_0. \end{cases} \tag{2}$$

It is obvious that the etching depth tailors the transverse index profile in the holey region. From Eq. (2), the index step Δn between the optical aperture ($r < R$) and the holey region ($r > R$) is given as $\gamma(n_{\rm a} + n_{\rm s})/2$. Thereby the index step Δn is related merely to the factor γ, and the deeper etching caused the larger index step Δn.

There were 4 degrees of freedom (R, r_0, L, θ or N) in the petal-shape holey structure. Herein three parameters: R, r_0, and L, are fixed, whereas the hole number N is varied. The lager hole number N means the smaller lateral dimension for each etched hole. In the fabrication process, all the samples are etched at the same time. Since the etching depth strongly depends on the lateral dimension of the annular-sector-shaped hole, the larger hole number N leads to a shallower etching depth for the same etching time, which corresponds to the smaller γ-factor.[52] At the same time, the smaller index step Δn is obtained. On the other hand, along the radial direction outwards from the centre in the top DBR, the lateral dimension is gradually increased in each annular-sector-shaped hole, and the factor γ is also gradually increased along the radial direction outwards from the centre. Thus the factor γ is a function of radius r, and the index profile is graded along the radial direction outwards from the centre in the holey region. The schematic of the effective index profile is shown in Fig. 1(b). When the hole number N is smaller, the index step Δn is larger, and the stronger index confinement is achieved. The stronger index confinement reduces the mode size, yielding less diffraction loss. In addition, the holes introduced into the top DBR reduce the reflectivity of the DBR and increase the scattering loss and the mirror reflection loss in the holey region. When the hole number N is larger, the scattering loss and the mirror reflection loss become larger. The diffraction loss also becomes larger because of the lower index step Δn and the graded index profile in the holey region. Thus the larger hole number N leads to a larger total loss. As a result, the larger N and deeper etching are beneficial to filtering the higher-order modes. Single-mode holey VCSELs can be easily realized with the larger hole number N.

3. Fabrication

The 850-nm GaAs-based VCSEL epilayer structure is studied. The epilayer wafer is produced by IQE Company, and is comprised of a triple GaAs quantum-well active layer, an $Al_{0.98}Ga_{0.02}As$ p-side oxide layer, lower 34.5-pair n-type and upper 20.5-pair p-type $Al_{0.12}Ga_{0.88}As/Al_{0.9}Ga_{0.1}As$ DBRs, and a top p-GaAs contact layer. Mesa structures with a diameter of 86 μm were formed on the epilayer structure mentioned above by the optical lithography and

wet etch method. The $Al_{0.98}Ga_{0.02}As$ layer was exposed to yield the oxide aperture with a diameter of 20 μm, which was larger than the optical aperture, and was followed by SiO_2 passivation. After opening the SiO_2 layer, a p-type metal (Ti–Au) contact was deposited. Subsequently, the petal-shape holey pattern was defined using the electron beam resist (ZEP520A) by an electron beam writing system (Raith 150), and the holes were etched down by the inductively coupled plasma (ICP) etching system (Oxford 100) with Cl_2/BCl_3 serving as the etching gases. Finally, the substrate was thinned, and an n-type (Au–Ge–Ni–Au) Ohmic contact was evaporated on the substrate. The scanning electron microscope (SEM) image is shown in Fig. 1(c).

We have fabricated and measured four types of device structures, i.e., structures A ($N = 5$), B ($N = 6$), C ($N = 9$) and D ($N = 10$). In the dry etching process, all the samples were etched for the same time. Since the etching depth strongly depends on the lateral dimension of the annular-sector-shape hole, the larger hole number N leads to the shallower etching depth under the condition of the same etching time. After the etching process, the etching depths for the four types were 1.9 μm (A), 1.6 μm (B), 1.3 μm (C), and 1.1 μm (D). Hence the smallest index step Δn was obtained in the D-type device according to Eq. (2). For comparison, the conventional VCSEL without the holey structure of the same oxide aperture in the top DBR was also fabricated on the same wafer.

4. Results and discussion

4.1. Output power and modal characteristics

All the devices were measured under a continuous-wave (CW) current at room temperature (RT). Figure 2 shows light–current–voltage (L–I–V) curves. The output power and the slop efficiency of VCSEL with a holey structure are reduced, whereas the threshold current is increased compared with those of the conventional oxide-confined VCSEL. Furthermore, the threshold current of holey VCSEL increases and the slop efficiency reduces with the hole number N increasing. These characteristics are attributed to the larger loss introduced by etched holes. With the hole number N increasing, the total loss increases and higher current needs to provide sufficient gain for lasing. Thus the slope efficiency decreases and the threshold current increases as the hole number N is increased. Additionally, with the hole number N increasing, the field profile becomes more extended owing to the shallow etching and the graded index profile. The loss for the lasing modes increases and the output power reduces as the annular-sector-shaped hole number N is increased. For example, single-mode output powers for types C and D are both about 1 mW.

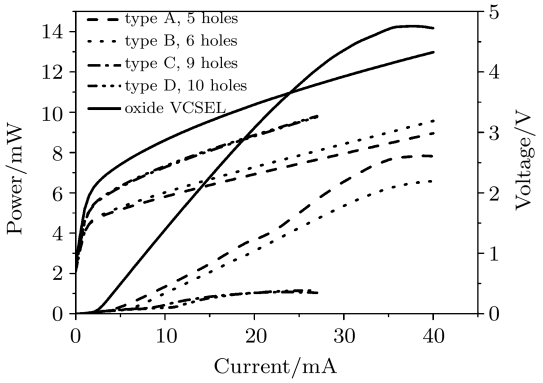


Fig. 2. The L–I–V curves of four structures and conventional oxide-confined VCSEL, all with the same oxide apertures and no etched patterns.

Figure 3(a) demonstrates the spectrum of the conventional oxide-confined VCSEL at 9 mA. The device operates in multiple modes, because of the large oxide aperture. Figure 3(b) shows the spectral characteristics of the four types, which are measured by an optical spectrum analyser (Agilent 86142B, Resolution 0.06 nm) under RT. Among the four types, types A and B operate in multiple modes. However, types C and D operate in single mode even at rollover. The side mode suppression ratio (SMSR) exceeds 30 dB throughout the entire drive current range. For the measured devices, because the size of the optical aperture is larger than that of the oxide aperture, the separated confinement is implemented. The holey pattern overlaps the oxide aperture by 4 μm, and the fundamental mode and the higher-order modes all suffer considerable losses in the four types. Typically, the mode sizes of the higher-order modes are larger than that of the fundamental mode. Thus the higher loss for the higher-order modes was achieved in the petal-shaped holey structure with a larger hole number N. Due to the insufficient gain, the higher-order modes are suppressed. The lasing spectra are purified and the single-mode operation is achieved.

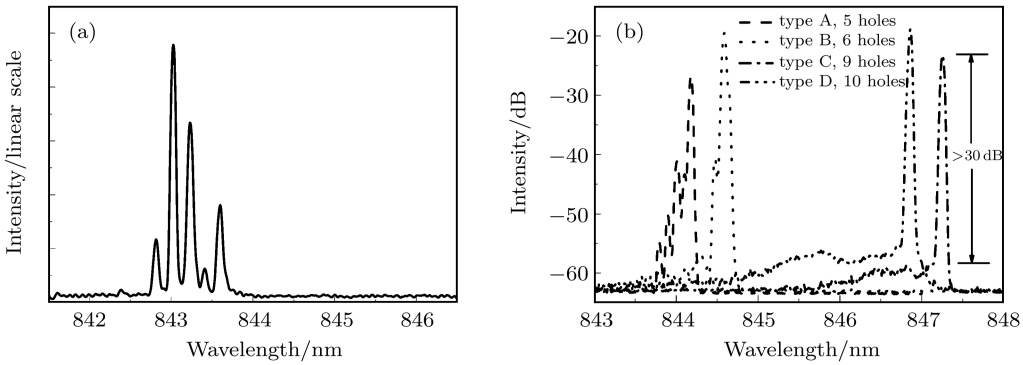


Fig. 3. (a) Spectrum of the conventional oxide-confined VCSEL at 9 mA, and (b) measured spectral characteristics of the four types. The CW currents for types A, B, C and D are 9 mA, 15 mA, 27 mA and 26 mA, respectively.

4.2. Far field patterns

The far field patterns (FFPs) of single-mode devices are also measured under room temperature. Because of the multi-mode operation, the FFPs of the conventional oxide-confined VCSEL with no etched holes are of ring shape, non-Gaussian distribution, which are shown in Fig. 4. Figures 5(a) and 5(b) show the FFPs of types A and B, respectively. Different from the FFPs of the conventional oxide-confined multi-mode VCSEL, the FFPs are of Gaussian distribution over the entire drive current range, although the two devices operated in multiple modes. This effect is probably attributed to the graded index profile. The Gaussian distribution FFPs of multi-mode holey VCSELs indicate that the single-fundamental-mode characteristic cannot be confirmed only by the Gaussian distribution FFPs without the optical spectrum measurement, contrary to the results reported in Ref. [53] where the single-fundamental-mode operation was confirmed only by the narrowed Gaussian FFPs. The average divergence angle (averaging the divergence angles in the x and the y directions; divergence angle that is defined as the full width at half maximum (FWHM) of the FFPs) of type A increases linearly as the current increases, whereas the average divergence angle of type B also approximately linearly changes. The shallower etching depth reduces the divergence angle of the multi-mode holey VCSEL, which can be seen by comparing Fig. 5(a) with Fig. 5(b). The FFPs of types C and D are shown in Fig. 6. The far field profiles are

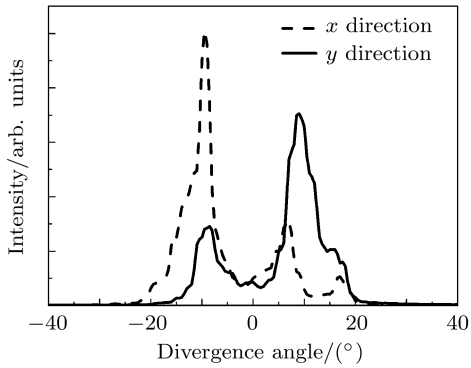


Fig. 4. Typical FFPs of the conventional oxide-confined VCSEL, measured in the x and the y directions at CW current of 9 mA.

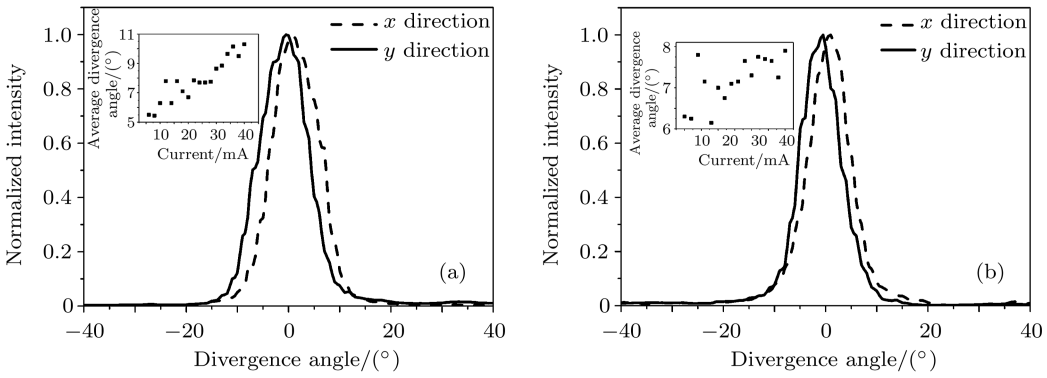


Fig. 5. Measured FFPs. (a) Type A. The FFPs are measured in the x and the y directions at CW current of 35 mA. The inset shows the divergence angles over the entire drive current range. (b) Type B. The FFPs are measured in the x and the y directions at CW current of 40 mA. The inset shows the divergence angles over the entire drive current range.

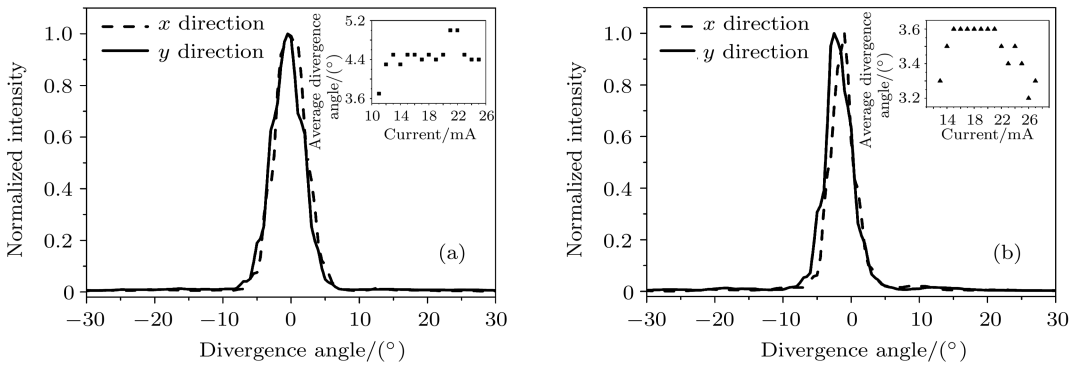


Fig. 6. (a) Type C. The FFPs are measured in the x and the y directions at a continuous wave current of 25 mA. The inset shows the average divergence angles over the entire drive current range. (b) Type D. The FFPs are measured in the x and the y directions at a continuous wave current of 26 mA. The inset shows the average divergence angles over the entire drive current range.

of Gaussian distribution throughout the entire drive current range. The average divergence angles of type C over the entire drive current range, which are calculated by averaging the divergence angles in the x and the y directions, are between 4.3° and 4.5°. However, the average divergence angles of type D remain in a range of 3.2°–3.6° throughout the entire drive current range. The stable FFPs result from the low differential resistance (about 45 Ω) induced by the large oxide aperture.

The lowest measured divergence angle is also less than the result (5.1°) reported in Ref. [37], in which the reduced divergence angle was realized by introducing a photonic crystal waveguide inducing the low index step Δn between the optical aperture and the holey region in the top DBR. However, for the petal-shape holey structure, two main features make contributions to the high-quality beams. The first one is of the graded index distribution in the top DBR, introduced by the etched holes. In our previous work, we reported that the index step Δn between the optical aperture and the holey region steered the FFP, and the larger index step Δn led to the higher divergence angle.[37] However, as mentioned above, due to the enlarged lateral dimension of the hole along the radial direction outwards from the centre, the hole depth gradually increases, and the index step Δn also increases gradually. The graded index profile in the top DBR widens the optical field, and the narrow beam divergence is achieved, because the FFP is obtained by Fourier transform of the near field pattern. The other one is of the shallow etching, which makes contribution to the low index step Δn between the optical aperture and the holey region. With the hole number N increasing, the etching depth reduces under the condition of the same etching time.

4.3. Coupling efficiency

The coupling efficiencies into a multi-mode fibre are measured at CW current under RT. Coupling is implemented with no optics by simple butt-coupling into the flat-cut uncoated fibre (62.5-μm step index fibre with 0.275 in numerical aperture and 5 m in length). Coupling loss depends on lateral displacement, longitudinal displacement, tilt, and axial rotation.[54] The experimental results are demonstrated in Fig. 7. For type A, the coupling efficiency

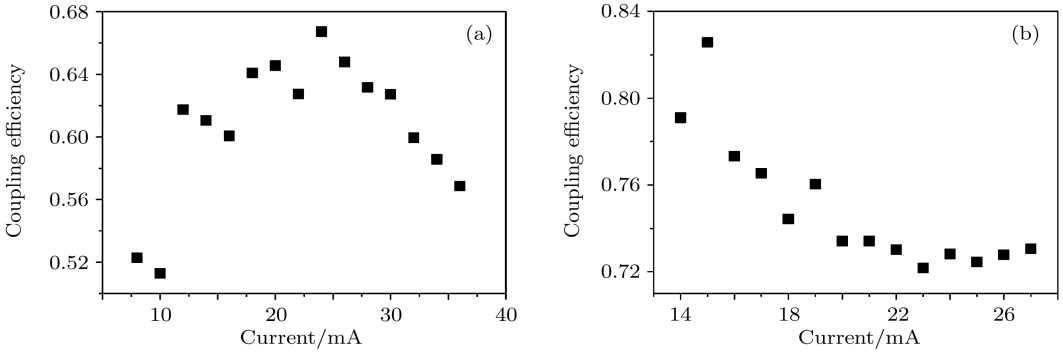


Fig. 7. Coupling efficiencies into a multi-mode fibre at different currents. (a) Type A. (b) Type D.

increases to 67% and then reduces with the injected current increasing, because VCSEL-fibre coupling efficiency into multi-mode fibre strongly reduces with the increase of transverse mode number for strongly index guided VCSEL.[55] The coupling efficiency reduces from 82% to 72% as the injected current increases for type D. After correction for the 4% Fresnel loss at the output end of the fibre with neglecting the transmission loss, the maximum coupling efficiency reaches 86%. The relatively high coupling efficiency is attributed to the single-fundamental-mode characteristic. The conventional oxidized VCSEL has a little power coupled into the fibre, and the coupling efficiency is less than 5% in our experiment, because of the inferior mode matching.[55]

5. Conclusions

VCSELs with petal-shape holey structures are demonstrated. The area-weighted average refractive index model is used to obtain the effective index distribution in the holey region. The index step between the optical aperture and the holey region is deduced from the model, which is related merely to the etching depth. Experimental results show that the beam quality of the holey VCSEL was improved in comparison with that of conventional oxide-confined VCSEL. The multi-mode holey VCSELs possess Gaussian far-field profiles throughout the entire current range, which is probably due to the graded index profile. With the hole number increasing, the holey VCSEL operates in a single fundamental mode (SMSR $>$ 30 dB), and its far-field pattern is of Gaussian distribution, with the divergence angle further reduced. The single-mode characteristic is attributed to the large total loss, and the high-quality beam is due to the graded index profile and the shallow etching in the top DBR. However, the maximum output power of single-mode holey VCSEL is about 1 mW due to the large loss induced by etched holes. In order to improve the single-mode power and suppress higher-order modes, the optical aperture can be enlarged appropriately in holey VCSEL with a large hole number (for example, $N = 9$ or 10). Thus single-mode operation may be obtained, and the higher output power with the high-quality beam can be expected.

The low divergence beam enhances the coupling efficiency into the fibre. The maximum coupling efficiency into a multi-mode fibre reaches 86% for the single-mode device in our experiment. Besides, we believe that these multi-mode holey VCSELs with Gaussian distributed far-field patterns are good candidates for the laser printing for the demands of high power and Gaussian-like beam profile in the application of the laser printing.[6]

References

[1] Iga K, Koyama F and Kinoshita S 1988 *IEEE J. Quantum Electron.* **24** 1845

[2] Wu J and Summers H D 2010 *Chin. Phys.* B **19** 014213

[3] Yang H, Guo X, Guan B L, Wang T X and Shen G D 2008 *Acta Phys. Sin.* **57** 2959 (in Chinese)

[4] Li H Q, Zhang J, Cui D F, Xu Z Y, Ning Y Q, Yan C L, Qin L, Liu Y, Wang L J and Cao J L 2004 *Acta Phys. Sin.* **53** 2986 (in Chinese)

[5] Tong C Z, Niu Z C, Han Q and Wu R H 2005 *Acta Phys. Sin.* **54** 3651 (in Chinese)

[6] Mukoyama N, Otoma H, Sakurai J, Ueki N and Nakayama H 2008 *Proc. SPIE* **6908** 69080H1

[7] Rao Z, Matteo J A, Hesselink L and Harris J S 2006 *Proc. SPIE* **6132** 61320J1

[8] Szweda R 2006 *III-Vs REVIEW* **19** 32

[9] Giannopoulos A V, Kasten A M, Long C M, Chen C and Choquette K D 2008 *Appl. Opt.* **47** 4555

[10] Ortsiefer M, Hofmann W, Rönneberg E, Boletti A, Gatto A, Boffi P, Rosskopf J, Shau R, Neumeyr C, Böhm G, Martinelli M and Amann M C 2008 *Electron. Lett.* **44** 974

[11] Wiedenmann D, King R, Jung C, Jäger R, Michalzik R, Schnitzer P, Kicherer M and Ebeling K J 1999 *IEEE J. Select. Topics Quantum Electron.* **5** 503

[12] Lin C K, Tandon A, Djordjev K, Corzine S W and Tan M R T 2007 *IEEE J. Select. Topics Quantum Electron.* **13** 1332

[13] Zappe H P, Hess M, Moser M, Hövel R, Gulden K, Gauggel H P and Sopra di F M 2000 *Appl. Opt.* **39** 2475

[14] Cattaneo H and Hernberg R 2005 *Appl. Opt.* **44** 6593

[15] Serkland D K, Peake G M, Geib K M, Lutwak R, Garvey R M, Varghese M and Mescher M 2006 *Proc. SPIE* **6132** 6132081

[16] Knappe S, Shah V, Schwindt P D D, Hollberg L, Kitching J, Liew L A and Moreland J 2004 *Appl. Phys. Lett.* **85** 1460

[17] Chang-Hasnain C J 2003 *IEEE Opt. Commun.* S30–S34

[18] Amann M C and Hofmann W 2009 *IEEE J. Select. Topics Quantum Electron.* **15** 861

[19] Leisher P O, Danner A J and Choquette K D 2006 *IEEE Photon. Technol. Lett.* **18** 2156

[20] Onishi Y, Saga N, Koyama K, Doi H, Ishizuka T, Yamada T, Fujii K, Mori H, Hashimoto J, Shimazu M, Yamaguchi A and Katsuyama T 2009 *IEEE J. Select. Topics Quantum Electron.* **15** 838

[21] Kapon E and Sirbu A 2009 *Nature Photon.* **3** 27

[22] Dallesasse J M, Holonyak N, Sugg A R, Richard T A and El-Zein N 1990 *Appl. Phys. Lett.* **57** 2844

[23] Lear K L, Choquette K D, Schneider R P and Kilcoyne S P 1995 *Appl. Phys. Lett.* **66** 2616

[24] Choquette K D, Geib K M, Ashby C I H, Twesten R D, Blum O, Hou H Q, Follstaedt D M, Hammons B E, Mathes D and Hull R 1997 *IEEE J. Select. Topics Quantum Electron.* **3** 916

[25] Satuby Y and Orenstein M 1998 *IEEE Photon. Technol. Lett.* **10** 760

[26] Leisher P O, Danner A J, Raftery Jr J J and Choquette K D 2005 *Electron. Lett.* **41** 1010

[27] Yang H P D, Lai F I, Chang Y H, Yu H C, Sung C P, Kuo H C, Wang S C, Lin S Y and Chi J Y 2005 *Electron. Lett.* **41** 326

[28] Weigl B, Grabherr M, Michalzik R, Reiner G and Ebeling K J 1996 *IEEE Photon. Technol. Lett.* **8** 971

[29] Lim D H, Hwang S M and Nam S H 2001 *14th Annual Meeting of the IEEE Lasers and Electro-Optics Society* **2** 724

[30] Martinsson H, Vukŭsić J A, Grabherr M, Michalzik R, Jäger R, Ebeling K J and Larsson A 1999 *IEEE Photon. Technol. Lett.* **11** 1536

[31] Haglund Å, Gustavsson J S, Vukŭsić J, Modh P and Larsson A 2004 *IEEE Photon. Technol. Lett.* **16** 368

[32] Huang M C Y, Zhou Y and Chang-Hasnain C J 2007 *Nature Photon.* **1** 119

[33] Shinada S and Koyama F 2002 *IEEE Photon. Technol. Lett.* **14** 1641

[34] Ueki N, Sakamoto A, Nakamura T, Nakayama H, Sakurai J, Otoma H, Miyamoto Y, Yoshikawa M and Fuse M 1999 *IEEE Photon. Technol. Lett.* **11** 1539

[35] Ostermann J M, Rinaldi F, Debernardi P and Michalzik R 2005 *IEEE Photon. Technol. Lett.* **17** 2256

[36] Unold H J, Golling M, Michalzik R, Supper D and Ebeling K J 2001 *Proc. 27th Euro. Conf. Opt. Commun.* p. talk Th.A.1.4

[37] Liu A J, Xing M X, Qu H W, Chen W, Zhou W J and Zheng W H 2009 *Appl. Phys. Lett.* **94** 191105

[38] Liu A J, Xing M X, Qu H W, Chen W, Zhou W J and Zheng W H 2010 *Acta Phys. Sin.* **59** 1035 (in Chinese)

[39] Song D S, Kim S H, Park H G, Kim C K and Lee Y H 2002 *Appl. Phys. Lett.* **80** 3901

[40] Yang H P D, Hsu I C, Chang Y H, Lai F I, Yu H C, Lin G, Hsiao R S, Maleev N A, Blokhin S A, Kuo H C and Chi J Y 2008 *J. Lightw. Technol.* **26** 1387

[41] Romstad F, Bischoff S, Juhl M, Jacobsen S and Birkedal D 2008 *Proc. SPIE* **6908** 69080C1

[42] Stevens R, Gilet P, Larrue A, Grenouillet L, Olivier N, Grosse P, Gilbert K, Hladys B, Bakir B B, Berggren J, Hammar M and Chelnokov A 2008 *Proc. SPIE* **6997** 69970X1

[43] Kasten A M, Sulkin J D, Leisher P O, McElfresh D K, Vacar D and Choquette K D 2008 *IEEE J. Selet. Topics Quantum Electron.* **14** 1123

[44] Czyszanowski T, Dems M, Thienpont H and Panajotov K 2007 *Opt. Express* **15** 1301

[45] Young E W, Choquette K D, Chuang S L, Geib K M, Fischer A J and Allerman A A 2001 *IEEE Photon. Technol. Lett.* **13** 927

[46] Fischer A J, Chow W W, Serkland D K, Merman A A, Geib K M and Choquette K D 2001 *Conference on Lasers and Electro-Optics* (CLEO) p. talk CTuB1

[47] Chang K S, Song Y M and Lee Y T 2007 *Appl. Phys.* B **89** 231

[48] Furukawa A, Sasaki S, Hoshi M, Matsuzono A, Moritoh K and Baba T 2004 *Appl. Phys. Lett.* **85** 5161

[49] Leisher P O, Danner A J, Raftery Jr J J, Siriani D and Choquette K D 2006 *IEEE J. Quantum Electron.* **42** 1091

[50] Morito K, Mori D, Mizuta E and Baba T 2005 *Proc. SPIE* **5722** 191

[51] Yang H P D, Hsu I C, Lai F I, Kuo H C and Chi J Y 2006 *Jpn. J. Appl. Phys.* **45** L871

[52] Yokouchi N, Danner A J and Choquette K D 2003 *Appl. Phys. Lett.* **82** 1344

[53] Yokouchi N, Ueda N, Shinagawa T, Iwai N, Sasaki Y, Ariga M, Uchiyama S, Shiina Y and Kasukawa A 2001 *The 4th Pacific Rim Conference on Lasers and Electro-Optics* **2** II-586

[54] Ogura A, Kuchiki S, Shiraishi K, Ohta K and Oishi I 2001 *IEEE Photon. Technol. Lett.* **13** 1191

[55] Heinrich J, Zeeb E and Ebeling K J 1997 *IEEE Photon. Technol. Lett.* **9** 1555